Metasurface enabled On-Chip Generation and Manipulation of Vector Beams from Vertical Cavity Surface-Emitting Lasers

Pan Fu, Pei-Nan Ni, Bo Wu, Xian-Zhi Pei, Qiu-Hua Wang, Pei-Pei Chen, Chen Xu, Qiang Kan*,Wei-Guo Chu* and Yi-Yang Xie**

P. Fu, B. Wu, X. Z. Pei, Prof. C. Xu, Prof. Y. Y. Xie

Key Laboratory of Optoelectronics Technology

Ministry of Education

Beijing University of Technology

Beijing, 100124, China

E-mail: xieyiyang@bjut.edu.cn

Dr. P. N. Ni

Faculty of Engineering and Natural Science

Tampere University

Tampere 33720, Finland

E-mail: peinan.ni@tuni.fi

Dr. Q. H. Wang, Prof. Q. Kan

Key Laboratory of Semiconductor Materials Science,

Institute of Semiconductors, Chinese Academy of Sciences,

This article has been accepted for publication and undergone full peer review but has not been through the copyediting, typesetting, pagination and proofreading process, which may lead to differences between this version and the Version of Record. Please cite this article as doi: 10.1002/adma.202204286.

Beijing, 100083, China

E-mail: kanqiang@semi.ac.cn

Dr. P. P. Chen, Prof. W. G. Chu

Nanofabrication Laboratory, CAS Key Laboratory for Nanophotonic Materials and Devices, CAS Key Laboratory for Nanosystems and Hierarchical Fabrication,

CAS Center for Excellence in Nanoscience,

National Center for Nanoscience and Technology,

Beijing 100190, China.

E-mail: wgchu@nanoctr.cn

Keywords: Metasurface; Vector beams; VCSELs; on-chip integration

Abstract:

Metasurface polarization optics that consist of two-dimensional array of birefringent nano-antennas have proven remarkable capabilities to generate and manipulate vectorial fields with subwavelength resolution and high efficiency. Integrating this new type of metasurface with the standard VCSEL platform enables an ultracompact and powerful solution to control both phase and polarization properties of the laser on a chip, which allows to structure a VCSEL into vector beams with on-demand wavefronts. Here, we demonstrate this concept by directly generating versatile vector beams from commercially available VCSELs through on-chip integration of high-index dielectric metasurfaces. Experimentally, the versatility of our approach for the development of vectorial VCSELs are validated by implementing a variety of functionalities, including directional emission of multibeam with specified polarizations, vectorial holographic display, and vector vortex beams generations. Notably, the proposed vectorial VCSELs integrated with a single layer of beam shaping metasurface bypass the requirements of multiple cascaded optical components, and thus have the potential to promote the advancements of ultracompact, lightweight, and scalable vector beams

sources, enriching and expanding the applications of VCSELs in optical communications, laser manipulation and processing, information encryption, and quantum optics.

1. Introduction:

Structured light that refers to harnessing optical fields with spatially variant properties, such as the amplitude, phase, and polarization states, has stimulated the development of modern optical technologies during the past two or three decades with enormous interest for both fundamental science and technology.[1-3] The diverse spatial characteristics of structured beams have fueled a rapid growth of many fields, ranging from imaging, microscopy, metrology, and 3D optical sensing to quantum information processing and optical communications.[4-6] As one of the typical structured light, laser beams with spatially inhomogeneous polarization states, also called vector beams (VBs), exhibit intriguing features compared with the conventional homogeneously polarized scalar lasers. For instance, using a high numerical lens, a cylindrical vector beam of radial polarization can be tightly focused smaller than the diffraction limit with a strong and non-propagating longitudinal electric field at the focal plane, whereas a focused azimuthally polarized beam can create an axial magnetic field component without any electric field in its center.[7-8] Such unique polarization characteristics of VBs render them a powerful toolkit in a large variety of applications, including optical trapping and manipulations, polarization spectroscopy, laser processing, and high-resolution imaging, *etc*.[9-11] Moreover, the distinct correlation properties manifested in the spatial and polarization degrees of freedom of VBs that resemble quantum entanglement could be used in the prospects of quantum optics applications. Notably, the concepts associated with the singularity of either the angle of the polarization vector or the phase of the complex amplitude have made profound impacts even beyond optics, which has been significantly expanded to other research fields, such as electron and plasma beams.[12-13]

To unveil the full potential of VBs, it relies on the development of efficient VBs sources, which has been attracting intensive efforts to generate VBs based on different platforms, including in the free space,[14] optical fibers[15], and integrated devices[16]. Among them, the advantages of Vertical Cavity Surface-Emitting Lasers (VCSELs), such as circular beam profile, low power consumption and fabrication cost, high modulation speed, ease of two-dimensional array fabrications and optics integrations, *etc*,[17-18] are highly desirable and suitable to develop VB source. To date, the large number of methods that have been adopted for VBs generations can be mainly categorized into two kinds of active and passive schemes, respectively. In active methods, the laser structure is modified by placing optical elements inside the cavity such that the beam is favored and selected in a desired vector mode,[19-20] whereas such modification comes at the expense of introducing additional intracavity loss. By contrast, the passive methods can preserve the pristine laser structure by directly transforming the conventional Gaussian laser beam into the desired VB outside the cavity.[21-22] Therefore, the non-intrusive nature of the passive method makes it more flexible and attractive than the active one. In this context, important progresses have been achieved by externally coupling additional polarization or phase modulating components with VCSELs, such as frequency selective volume Bragg grating,[23] birefringent external cavity,[24] and liquid-crystal spatial light modulator,[25] *etc*. Nevertheless, such solutions are often bulky, complex, and require delicate alignments, which is against the current tendency toward to miniaturized photonic systems. Alternatively, on-chip generation of VBs without the need of external components stands out with the advantages of high efficiency, compactness, and robustness, which is preferred and more favorable for optoelectronic integrations. In this regard, a compact vector vortex source was demonstrated by fabricating metallic gratings, such as concentric gold rings, on top of the emitting surface of VCSELs to excite and select the surface plasmon polariton modes.[26] But the intrinsic Ohmic losses caused by the plasmonic structure raises wide concerns in terms of high-efficient operations.

Advances in high index dielectric metasurfaces that consist of two-dimensional array of lossless optical nano-resonators arranged in a subwavelength lattice constant enable exceptional controllability over the phase, amplitude, and polarization of the light with high efficiency and spatial resolution, which gives rise to a variety of compact optical devices in the free space.[27-29] In particular, the unique advantages of metasurface, such as planar configuration, ultra-compactness, and complementary metal oxide semiconductor (CMOS) compatibility, have gained wide popularity for on-chip applications.[30-32] Despite the recent achievements in shaping the wavefronts of VCSELs though integration of dielectric metasurfaces, such as tailoring the phase profile,[32-33] controlling the orbital angular momentum,[34-35] and splitting different circular polarization components,[36] arbitrary control of both the phase and polarization states of VCSELs using a single layer of integrated metasurface, which is the key for the generation of VBs on a chip, still remain elusive.

Here we report on-chip generation and manipulation of vector beams by exploiting integrated vectorial metasurfaces to simultaneously control the phase and polarization properties of a standard infrared VCSEL. Accordingly, birefringent metasurfaces are properly constructed by assembling meta-atoms that can operate both as nano phase-retarders and waveplates at the emitting surface of the VCSEL, which allows us to point-by-point encode versatile spatial variant phase profiles and polarization distributions into the local optical fields with subwavelength spatial resolution. Capitalizing on this concept, we demonstrate and discuss the versatility of our approach to structure the outgoing beams of VCSELs with diverse on-demand vectorial characteristics, including directional emission of multibeam with specified polarizations, vectorial holographic display, and vector vortex beams generations. The developed method paves the way to realize customized vector beams from the standard VCSELs platform, which could establish close connections in the vibrant fields of structured light, singular optics, metasurface, and semiconductor laser technology with promising application potentials.

2. Results:

2.1. On-chip control of phase and polarization states of VCSELs

Figure 1a represents a schematic illustration of the proposed monolithic integration of high index vectorial metasurface with a standard back-side emission VCSEL. (See Experimental Section for fabrication details) Prior to the integration of metasurface, the lasing characteristic of the fabricated VCSELs were investigated in detail. (See Fig. S1 Supplementary Information). As evidenced, the bare VCSELs exhibit good single-mode emission characteristics due to the deployed very small oxide aperture with a diameter of 3 μm in the design. The VCSELs were mounted onto a heat sink to minimize the thermal effect on the measurement, which helps to stabilize the lasing wavelength around 977 nm under different injected continuous-wave (CW) currents up to 5 mA. (See Fig. S1b Supplementary Information). As a result of the cylindrically symmetric cavity and isotropic gain, VCSELs typically emit linearly polarized laser along the [011] or $[0\bar{1}1]$ crystal axis. Accordingly, to avoid the polarization switching, the fabricated VCSELs were operated under small injection of current (<5 mA) such that the devices can exhibit TM-polarization dominated emissions during the measurement. (See Fig. S2 Supplementary Information). Note that such monochromatic lasing emissions with well-defined mode characteristics greatly facilitate the design of wavefront shaping metasurface. To control both the phase and polarization states of the VCSEL on a chip, GaAs nano-pillars with rectangular cross-sections were arranged in a subwavelength square lattice on the emitting surface of the laser. In this way, each of the nano-pillars servering as the building block of the integrated metasurface can be considered as a truncated waveguide with anisotropic effective refractive indices of the waveguide modes polarized along its fast and slow axis. (See the middle panel in Fig. 1a) Consequently, independent control of the propagation phase imposed to the orthogonally polarized light along these two axes can be achieved by changing its width (D_u) and length (D_v), respectively, which can be leveraged to manipulate both the local polarization states and

the phase retardance. Specifically, after the modulation by a birefringent metasurface, the outgoing beam (E_{out}) from the metasurface integrated VCSELs (Meta-VCSELs) with TM-polarized emission (E_{in}), can be expressed conveniently using the Jones Matrix ($J(\theta)$):

$$E_{out} = J(\theta) \cdot E_{in}, \quad (1)$$

$$\text{and } J(\theta) = R(\theta)^T \times \begin{bmatrix} t_u & 0 \\ 0 & t_v \end{bmatrix} \times R(\theta) \quad (2)$$

, where $t_u = T_u e^{i\varphi_u}$, and $t_v = T_v e^{i\varphi_v}$ are the complex transmission coefficients of the meta-atom along its fast and slow axes, respectively, $R(\theta) = \begin{bmatrix} cos\theta & -sin\theta \\ sin\theta & cos\theta \end{bmatrix}$ is a rotation matrix, ϑ is the rotation angle relative to the *x*-axis. (See the middle panel in Fig. 1a) This reveals that the linearly polarized beam of the VCSEL can be readily converted into any complex wavefront with on-demand phase profiles and polarization states by judiciously controlling the propagation phase, phase offset along the two orthogonal directions of the meta-atoms, and their orientation angles.

To prove this concept, in the first example, four rectangular nano-pillars with a fixed phase offset ($\delta\varphi = |\varphi_{u0} - \varphi_{v0}| = \pi$) between the two eigen-polarization channels and high transmission efficiency were employed as the building blocks to construct the integrated metasurface. **Fig. 1c** summarize the simulated complex transmission coefficients of the selected four meta-atoms when they are aligned with *x*-polarized light (ϑ = 0) at the lasing wavelength of 977 nm. Based on the selected meta-atoms, the continuous phase profile of a desired metasurface can be simply discretized into four phase levels with a constant step in the complete 2π phase range. By doing this, the outgoing beam (E_{out}) of the Meta-VCSEL can be rewritten as:

$$E_{out} = T_{u0} e^{i\varphi_{u0}} \cdot \begin{bmatrix} cos2\theta \\ sin2\theta \end{bmatrix} \quad (3)$$

As a result, the output beam will be imposed with a user-defined phase delay φ_{u0} while its polarization orientation can be rotated continuously by 2ϑ with respect to the original direction (referred as *x*-axis). In this case, each of the deployed meta-atoms actually functions as nano-half waveplate with phase controlling capability, which allow to locally imprint any phase functionality and linear polarization states along the equator of the Poincaré sphere at the emitting surface of VCSELs. (See the right panel of Fig. 1a)

It is worthy to stress that arbitrary polarization states with controllable phase can be realized from the Meta-VCSELs by operating the birefringent meta-atoms as other different types of nano waveplates, that is, by adjusting the phase difference $\delta\varphi$ to a specific value. For example, generations of elliptical polarizations have been demonstrated in the free space by using anisotropic meta-atoms with phase difference value $\delta\varphi$ equals to $\pi/2$.[37] Accordingly, in the second example, four meta-atoms with $\pi/2$ phase offset ($\delta\varphi$) were chosen to function as phase controlling nano-quarter waveplates (see Fig. 1d), which allows for the generation of elliptically polarized beams from VCSELs. For simplicity without loss of generality, we demonstrated that right-handed and left-handed circular polarization states can be directly generated from Meta-VCSELs by assembling the selected nano-quarter waveplates with a fixed rotation angle (ϑ) at 45^{o} and 135^{o}, respectively. We would like to emphasize that the capabilities to control both the phase and polarization of VCSELs enabled by the developed integration of metasurface polarization optics could unlock the potential to functionalize VCSELs in an ultracompact wafer-level fashion with previously unattainable vectorial properties.

2.2. Directional generation of multibeam with specified polarizations

The large refractive index of the dielectric metasurface is in favor of strong optical field confinement, wherein each meta-atom can be considered as a nearly isolated pixel with negligible dependence on

its neighboring elements. Taking this advantage, different beam functionalities can be multiplexed into the same metasurface through a simple design scheme of spatial multiplexing. Capitalizing on this concept, we develop a multi-sector Meta-VCSEL by dividing the integrated metasurface into a number of macroscopic areas such that it can collimate and split the emitting beam into a predefined array with specified deflection angles and polarization directions, as illustrated in **Fig. 2a**.

In this example, the integrated metasurface is constructed by arranging meta-atoms that operate as nano-half waveplates into four spatially segmented sub-arrays. The high accuracy and reliability of the developed nanofabrication processes for GaAs metasurfaces are revealed by the well-controlled shape and sidewall profiles of the integrated metasurface (see **Fig. 2b**), which are further confirmed by the good agreements between the simulated and measured transmission efficiency along the two orthogonal directions, respectively. (See Fig. S3 Supplementary Information). To implement collimated multi-beam splitting, each spatially divided sector of the metasurface is encoded with two superimposed phase functions:

$$\phi_{total} = \phi_{collimator} + \phi_{deflector} = 2\pi - \frac{2\pi n}{\lambda}\left(\sqrt{x^2 + y^2 + f^2} - f\right) - \frac{2\pi}{\lambda}x.\sin\theta_x - \frac{2\pi}{\lambda}y.\sin\theta_y \quad (4)$$

, where λ is the laser wavelength, n is the refractive index of the GaAs substrate, f is the focal length, θ_x and θ_y denote the deflection angle towards to x-axis and y-axis, respectively. Hence, the phase component $\phi_{collimator}$ will correct the diverging spherical wavefront of the original VCSEL beam for collimation purpose, while $\phi_{deflector}$ will further deflect the beam at a given angle. Meanwhile, the rotation angle $\theta_i(x, y)$ of the meta-atoms in the ith-section, where i =1, 2, 3, and 4 represents the section number, is set at 0°, 22.5°, 45°, and 67.5°, respectively, as depicted in Fig. 2b. According to *Equation 3*, the polarization direction of the beam modulated by each section will thus be rotated by $2\theta_i$ with respect to its initial direction (referred as x-polarization), respectively. In this way,

directional emissions of multi-beams with four specified linear polarizations, *i.e.,* 0^{o}, 45^{o}, 90^{o} and 135^{o}, can be realized from the proposed VCSEL, as illustrated in Fig. 2a.

The Meta-VCSELs were characterized using a home-built optical setup, in which an infrared CCD camera integrated with a microscope objective was mounted on a motorized linear translation stage to record the beam profiles of the laser in three directions (See Fig. S4 Supplementary Information). **Figure 2c** shows the intensity distribution of the outgoing beams measured along the propagation direction (*z*-direction), which reveals the generation of four well-collimated directional beams from the Meta-VCSEL. Moreover, the generated beams exhibit symmetric beam profile with comparable divergence angle. (See Fig. S5 Supplementary Information) The state of the polarizations (SOPs) of the beams were determined by the measurement of polarization-resolved intensity distributions in the *x*-*y* plane at *Z* = 1.5 cm using an additional polarizer, which show good agreement with the theoretical predictions (**Fig. 2d**). Likewise, the proposed segmented Meta-VCSEL can generate multibeams of arbitrary polarization states by operating the meta-atoms in each sector as other type of nano waveplates. For example, in combination of the use of the previously selected phase controlling nano half-waveplates and quarter-waveplates, we further demonstrate that multibeams with different linear polarizations and circular polarizations can be created from the developed Meta-VCSEL at the same time. (See Fig. S6 Supplementary Information)

2.3. On-chip vectorial holographic display

The versatility of the developed monolithic approach to structure a complex wavefront of the VCSEL is further validated by creating a vectorial holographic image with on-demand phase and polarization distributions. For this purpose, we divide the integrated metasurface hologram into four sectors, which are encoded independently to reconstruct the letters of “B”, “J”, “U”, and “T” with distinct and well-defined SOPs in the far field, respectively, as illustrated in **Fig. 3a and b**. Accordingly,

the phase distributions of the desired holograms were retrieved using the Gerchberg–Saxton algorithm, while the spatially resolved polarization conversions were realized by controlling the rotation angles (ϑ) of individual meta-atoms in each sector.

In experiment, the designed four letters can be observed simultaneously without any polarization analyzer (**Fig. 3c**), of which the pre-defined SOPs were further verified by adding a polarization analyzer rotated at different angles in the optical path. **Figure 3d** shows that each of the reconstructed letters, which corresponds to the pre-defined sector with a given SOP can be selectively concealed by filtering out the output polarization state using a polarizer, while exhibiting high extinction ratio to its counterpart image of orthogonal polarization. The above results validate the feasibility to realize on-chip vectorial holographic display using the developed Meta-VCSEL. However, a noticeable diverging spot was superimposed in the center of the holographic images, which indicates the unmodulated zero-order transmission. To evaluate the modulation efficiency of the metasurface in the current design, the percentage of the modulated light with respect to the total transmitted light was experimentally determined to be around 55% after passing through the metasurface, as discussed in Fig. S7. The efficiency of the designed metasurfaces is mainly limited by the non-unitary conversion efficiency of the selected nano waveplates and the few numbers of phase levels to discrete the phase profiles of the hologram, which can be further improved by using meta-atoms with higher efficiency and a finer phase step size. It is also worth noticing that the capability of the metasurface to precisely control the polarization states of the holographic images allows to eliminate the uncontrolled zero-order component through a simple polarization filtering, as demonstrated in Fig. S8. Furthermore, we show that vectorial holographic image that contains both linearly and circularly polarized information can be generated by operating the meta-atoms as nano half waveplates and quarter waveplates in the assigned sections, respectively. (See Fig. S9 Supplementary Information)

The above results prove the feasibility to realize on-chip vectorial holographic display that features compact, lightweight, and scalable holography systems by integrating metasurface holograms with a built-in semiconductor laser source. Since a vectorial holography can carry high-dimensional information rather than the simple scalar intensity information, combining vectorial holography with VCSELs allows to fully exploit their polarization degree of freedom as an additional information channel, which could substantially boost the capacity of VCSELs in optical communication, display, data storage, and optical encryption, *etc*.[38-39] We would like to stress that even though a rather simple segmented approach is employed in this work as a proof of the concept to demonstrate on-chip vectorial holography, other newly developed design strategies of vectorial metasurfaces, such as the interleaved methods,[40-41] and other non-interleaved methods to locally control the electric field vector of a pixelated metasurface,[42-43] can be readily implemented on the VCSELs platform, empowering the versatility of this new type of integrated vectorial holography system.

2.4. Generations of vector vortex beams

Vector vortex beams (VVBs) manifested as singularities in their space-variant polarizations can simultaneously carry spin and orbital angular momentum of light, promising their potential in wide areas, such as optical communication, optical manipulation, and laser processing, where conventional VCSELs that emit homogeneously polarized Gaussian beams are currently dominating. In particular, the orthogonality among VVBs provides a new basis of inherently infinite dimensions, which can be exploited to boost data capacity for addressing the unprecedented data growth and internet traffic. The capability of the integrated birefringent metasurface to locally encode arbitrary phase and polarization profiles at the emitting surface of a VCSEL through the combination of its unique phase and polarization response provides a feasible scheme for the generation of VVBs at an ultracompact wafer level. As a demonstration, meta-atoms that function as phase controlling nano

half waveplates were first assembled to construct vortex waveplates with different polarization orders, as shown in **Fig. 4a and b**. In this way, the typical scalar Gaussian beams of the VCSELs can be conveniently converted into cylindrical vector beams (CVBs) Moreover, to compensate the original diverging spherical wavefront of the VCSEL beam, a collimating phase profile $\phi_{collimator}$ was further imprinted onto the outgoing beams. Evidently, circular intensity distributions in the form of a doughnut like shape can be observed from the fabricated devices when no analyzer is used, indicating their polarization singularities in the central region. (**Fig. 4c**) As expected, the size of the central dark region grows as the value of the polarization order increases. The collimating behaviors of the generated beams were confirmed by the measurements of their intensity profiles along the propagation direction, which exhibit negligible divergence up to 4 mm. (See Fig. S10 Supplementary Information) The vectorial nature of these beams can be further confirmed by adding a polarizer in the optical path. Experimentally, petal-shaped intensity distributions resulting from the spatial resolved polarization profiles of the beams can be distinguished under the use of polarization analyzer. The observed two-lobe, four-lobe, and six-lobe patterns in orthogonal directions with respect to the transmission axis of the polarizer validate the generations of radial vector beams of *m* = 1, *m* = 2 and *m* = 3, respectively, as summarized in **Fig. 4 d**. The high contrast of the field lobes reveals the good polarization purity of the generated CVBs. The spatially variant polarization distributions of the output beams are further revealed by recording the variation of the intensity profiles when the polarizer is rotated continuously (See Movie S1-S2 Supplementary Information for details). In addition, by changing the initial phase of the metasurface vortex waveplates from $\varphi = 0$ to $\frac{\pi}{2}$, azimuthal vector beams can be generated from the Meta-VCSELs, as shown in Fig. S11. Moreover, vortex beams of other polarization states can be realized by operating the meta-atoms as different type of waveplate. For example, generations of circular spin angular momentum states combined with different orbital angular momentum states (*l* = 1, 2, and 3) were further

demonstrated by imposing helical wavefronts with user-defined topological charges to the VCSELs emissions using quarter-waveplate meta-atoms. (See Fig. S12 Supplementary Information).

We would like to stress that compared with other phase controlling elements, such as microscale spiral phase plates (SPPs),[44] integrating polarization metasurfaces with VCSELs enables a new type of on-chip vortex beam source with several advantages. Firstly, the unique controllability of vectorial metasurface over the phase and polarization states allow us to exploit chiral control of both spin angular momentum and OAM degrees of freedom of light at the same time, which will open exciting opportunities for new applications.[45] Secondly, the ultra-high spatial resolution of the metasurface is beneficial to create vortex beams with high mode purity. Given that high mode purity over 80% has been experimentally realized from SPPs integrated VCSELs that use eight phase levels,[44] we further disclose that the purity of a vortex VCSEL can be considerably improved by employing more meta-atoms levels in the design of metasurface, thanks to its advantageous subwavelength spatial resolution. (See Fig. S13 Supplementary Information). Thirdly, the CMOS compatibility and planar configuration of metasurfaces greatly facilitate their on-chip integrations with VCSELs, especially desirable for the fabrication of 2D array of vortex VCSELs in large scale. Last but not the least, the performance of the proposed Meta-VCSELs would significantly benefit from the fast-evolving active metasurface technologies, which enable remarkable control of light in real time.[46] We can envision that integrating this new class of active metasurface with VCSELs will empower generations of vortex beams with unprecedentedly tunable and controllable beam functionality and quality.

3. Discussion and Conclusion:

Controlling the phase and polarization states of the VCSEL with on-demand characteristics not only paves the way to generate customized VBs with versatile functionalities, but also serves as an essential piece to promote the thriving applications of VCSELs, which have been profoundly

extended from the traditional areas in optical communications, instrumentation, laser manufacturing, to a broader range of emerging fields, such as consumer electronics, frequency combs, and light detection and ranging (LiDAR) system, *etc*. For instance, proper phase corrections are required to mitigate the strong diffraction caused by the small emission aperture of VCSELs. Otherwise, the large divergence angle of a VCSEL beam (usually larger than 10^{o}) will severely impair its efficiency to couple with the optical system, such as the optical fibers and waveguide. On the other hand, due to their homogenous optical gain and polarization independent DBRs mirrors, controlling the polarization states of VCSELs usually relies on exquisite strategies to avoid interference with other laser characteristics. Notably, the unique wafer-level controllability over both phase and polarization of light enabled by a single layer of vectorial metasurface could provide a feasible and practical solution to overcome the aforementioned challenges, which can outperform the conventional bulky and heavy optical components with unmatched compactness and subwavelength spatial resolution.

To conclude, on-chip generation and manipulation of vector beams are achieved on the standard VCSEL platform by exploiting the optoelectronic integration of vectorial metasurfaces. The developed approach enables a powerful tool to structure the complex wavefronts of VCSELs in an ultracompact way, providing the access to previously unattainable phase and polarization degrees of freedom. Capitalizing on this concept, integrated metasurface polarization optics was constructed by assembling high index dielectric meta-atoms that function as phase controlling nano waveplates, which allows to point-by-point imprint the local fields of a VCSEL beam with on-demand phase profile and polarization distributions. The versatility of this approach is validated by structuring the outgoing beams of VCSELs with diverse vectorial characteristics, including directional emission of multibeam with specified polarizations, vectorial holographic display, and vector vortex beams

generations. The results open a novel avenue to realize compact, lightweight, and scalable vector beam sources bypassing the requirement of multiple cascaded optical components.

Experimental methods:

Numerical simulations. The light transmission from the meta-atoms were numerically investigated by the full-wave finite-difference time-domain (FDTD) approach. For the simplicity of fabrication, the height of meta-atoms was fixed at 700 nm. To retrieve the phase and amplitude of the light modulated by the integrated metasurface, GaAs nanopillars with identical rectangular cross-section were assembled on a GaAs bulk substrate in a subwavelength lattice constant of 350 nm. Accordingly, periodic boundary conditions are used along in-plane directions and perfectly matched layer (PML) boundary condition is applied along the light propagation in the FDTD simulations. To select the desired meta-atoms for the construction of metasurface, the meta-elements library was created by parameter sweeping of the GaAs nanopillar along its two orthogonal directions, as depicted in Fig. 1a.

On-chip integration of metasurface. A commercially available near-infrared VCSEL wafer. consisting of 30.5 pairs of top *p*-type distributed Bragg reflectors (DBRs), 28 pairs of bottom *n*-type DBRs, and 3 layers of quantum wells as the active region, was processed into back-side emission configuration. A small oxide aperture of 3 μm diameter is obtained by selectively oxidating a 30 nm $Al_{0.98}Ga_{0.02}As$ oxidation layer, which was sandwiched between the active region and top DBRs to ensure both optical and electrical confinement. As a result, state single mode operation was maintained during the optical characterization (See Fig. S1 Supplementary Information). After the metallization of the VCSELs, metasurfaces were directly integrated onto the back-side surface of the GaAs substrate by nano-fabricating the GaAs substrate into nanopillars. Specifically, a 180 nm thick Hydrogen silsesquioxane (HSQ) layer was spin-coated onto the substrate and defined into the metasurface

patterns using an Electron beam lithography system (EBL) with the acceleration voltage of 100 kV and the dose of 5000μC/cm^2. After developing in 1% (mass percentage) NaOH aqueous solution for 60 sec, the exposed resist will be turned into SiO_2 due to the chemical reaction to serve as the hard mask. To further transfer the defined metasurface patterns into the GaAs substrate, ICP-RIE etching using $SiCl_4/Cl_2$ (gas) is carried under optimized conditions (RF power:150W, microwave power: 250W, chamber presser: 8.0 Pa) to minimize the surface damage. Due to the lack of an etch-stopping layer in the current design of the laser structure, the etching rate has been carefully calibrated as 4 nm/s. In this way, the etching depth was solely adjusted by controlling the etching time.

Supporting Information

Supporting Information is available from the Wiley Online Library or from the author.

Acknowledgements

P. F. and P. N. N. contribute equally to this work. We acknowledge the financial support from the National Key R&D Program of China (2018YFA0209000), National Natural Science Foundation of China (62074011, 61604007, 61874145, 61774175), the Beijing Natural Science Foundation (4172009, 4182012), and Beijing Nova Program (No. Z201100006820096). The authors acknowledge the Nanofabrication Laboratory at National Centre for Nanoscience and Technology for sample fabrication.

Conflict of Interest

The authors declare no conflict of interest.

Data Availability Statement

The data that support the findings of this study are available from the corresponding author upon reasonable request.

Received: ((will be filled in by the editorial staff))
Revised: ((will be filled in by the editorial staff))
Published online: ((will be filled in by the editorial staff))

References

[1] A. H. Dorrah, F. Capasso, *Science* **2022**, 376, eabi6860.

[2] A. Forbes, M. de Oliveira, M. R. Dennis, *Nature Photonics* **2021**, 15, 253.

[3] E. Miyai, K. Sakai, T. Okano, W. Kunishi, D. Ohnishi, S. Noda, *Nature* **2006**, 441, 946.

[4] K. Jana, K. Herperger, F. Kong, Y. Mi, C. Zhang, P. Corkum, S. Sederberg, *Nature Photonics* **2021**, 15, 622.

[5] D. Lin, J. Carpenter, Y. Feng, S. Jain, Y. Jung, Y. Feng, M. N. Zervas, D. J. Richardson, *Nature communications* **2020**, 11, 1.

[6] V. D'Ambrosio, G. Carvacho, I. Agresti, L. Marrucci, F. Sciarrino, *Physical Review Letters* **2019**, 122, 013601.

[7] K. Kitamura, K. Sakai, S. Noda, *Optics express* **2010**, 18, 4518.

[8] J. Gao, S. Yan, Y. Zhou, G. Liang, Z. Zhang, Z. Wen, G. Chen, *Optica* **2021**, 8, 984.

[9] T. Bauer, S. Orlov, U. Peschel, P. Banzer, G. Leuchs, *Nature Photonics* **2014**, 8, 23.

[10] Z. Chen, T. Zeng, B. Qian, J. Ding, *Optics express* **2015**, 23, 17701.

[11] Y. Zhang, J. Shen, C. Min, Y. Jin, Y. Jiang, J. Liu, S. Zhu, Y. Sheng, A. V. Zayats, X. Yuan, *Nano letters* **2018**, 18, 5538.

[12] H. Lourenço-Martins, D. Gérard, M. Kociak, *Nature Physics* **2021**, 17, 598.

[13] V. Berezhiani, S. Mahajan, Z. Yoshida, M. Pekker, *Physical Review E* **2002**, 65, 046415.

[14] C. Rosales-Guzmán, N. Bhebhe, A. Forbes, *Optics express* **2017**, 25, 25697.

[15] S. Ramachandran, P. Kristensen, M. F. Yan, *Optics letters* **2009**, 34, 2525.

[16] Y. Chen, K.-Y. Xia, W.-G. Shen, J. Gao, Z.-Q. Yan, Z.-Q. Jiao, J.-P. Dou, H. Tang, Y.-Q. Lu, X.-M. Jin, *Physical Review Letters* **2020**, 124, 153601.

[17] C. J. Chang-Hasnain, Y. Zhou, M. C. Huang, C. Chase, *IEEE Journal of Selected Topics in Quantum Electronics* **2009**, 15, 869.

[18] A. Larsson, *IEEE Journal of selected topics in quantum electronics* **2011**, 17, 1552.

[19] Y. Mushiake, K. Matsumura, N. Nakajima, *Proceedings of the IEEE* **1972**, 60, 1107.

[20] J.-l. Li, K.-i. Ueda, M. Musha, A. Shirakawa, Z.-m. Zhang, *Optics letters* **2007**, 32, 1360.

[21] R. Dorn, S. Quabis, G. Leuchs, *Physical review letters* **2003**, 91, 233901.

[22] K. C. Toussaint, S. Park, J. E. Jureller, N. F. Scherer, *Optics letters* **2005**, 30, 2846.

[23] J. Jimenez-Garcia, P. Rodriguez, T. Guillet, T. Ackemann, *Physical review letters* **2017**, 119, 113902.

[24] Y. Kozawa, Y. Nara, N. Jikutani, Y. Higashi, S. Sato, *Optics Letters* **2018**, 43, 5659.

[25] J. Wang, J.-Y. Yang, I. M. Fazal, N. Ahmed, Y. Yan, H. Huang, Y. Ren, Y. Yue, S. Dolinar, M. Tur, *Nature photonics* **2012**, 6, 488.

[26] L. Cai, J. Zhang, W. Bai, Q. Wang, X. Wei, G. Song, *Applied Physics Letters* **2010**, 97, 201101.

[27] A. Arbabi, Y. Horie, M. Bagheri, A. Faraon, *Nature nanotechnology* **2015**, 10, 937.

[28] S. Wang, P. C. Wu, V.-C. Su, Y.-C. Lai, M.-K. Chen, H. Y. Kuo, B. H. Chen, Y. H. Chen, T.-T. Huang, J.-H. Wang, *Nature nanotechnology* **2018**, 13, 227.

[29] R. Sawant, P. Bhumkar, A. Y. Zhu, P. Ni, F. Capasso, P. Genevet, *Advanced Materials* **2019**, 31, 1805555.

[30] A. Leitis, M. L. Tseng, A. John-Herpin, Y. S. Kivshar, H. Altug, *Advanced Materials* **2021**, 33, 2102232.

[31] Z. Wang, T. Li, A. Soman, D. Mao, T. Kananen, T. Gu, *Nature communications* **2019**, 10, 1.

[32] Y.-Y. Xie, P.-N. Ni, Q.-H. Wang, Q. Kan, G. Briere, P.-P. Chen, Z.-Z. Zhao, A. Delga, H.-R. Ren, H.-D. Chen, *Nature nanotechnology* **2020**, 15, 125.

[33] Q. H. Wang, P. N. Ni, Y. Y. Xie, Q. Kan, P. P. Chen, P. Fu, J. Deng, T. L. Jin, H. D. Chen, H. W. H. Lee, *Laser & Photonics Reviews* **2021**, 15, 2000385.

[34] M. S. Seghilani, M. Myara, M. Sellahi, L. Legratiet, I. Sagnes, G. Beaudoin, P. Lalanne, A. Garnache, *Scientific reports* **2016**, 6, 1.

[35] P. Fu, P. N. Ni, Q. H. Wang, Y. F. Liu, B. Wu, P. P. Chen, Q. Kan, S. P. Wang, H. D. Chen, C. Xu, *Advanced Optical Materials* **2021**, 9, 2101308.

[36] D. Wen, J. Meng, J. J. Cadusch, K. B. Crozier, *Advanced Optical Materials* **2021**, 9, 2001780.

[37] F. Ding, B. Chang, Q. Wei, L. Huang, X. Guan, S. I. Bozhevolnyi, *Laser & Photonics Reviews* **2020**, 14, 2000116.

[38] Q. Song, X. Liu, C.-W. Qiu, P. Genevet, *Applied Physics Reviews* **2022**, 9, 011311.

[39] I. Kim, J. Jang, G. Kim, J. Lee, T. Badloe, J. Mun, J. Rho, *Nature communications* **2021**, 12, 1.

[40] Q. Song, A. Baroni, R. Sawant, P. Ni, V. Brandli, S. Chenot, S. Vézian, B. Damilano, P. de Mierry, S. Khadir, *Nature communications* **2020**, 11, 1.

[41] Z.-L. Deng, J. Deng, X. Zhuang, S. Wang, T. Shi, G. P. Wang, Y. Wang, J. Xu, Y. Cao, X. Wang, *Light: Science & Applications* **2018**, 7, 1.

[42] Z. H. Jiang, L. Kang, T. Yue, H. X. Xu, Y. Yang, Z. Jin, C. Yu, W. Hong, D. H. Werner, C. W. Qiu, *Advanced Materials* **2020**, 32, 1903983.

[43] E. Arbabi, S. M. Kamali, A. Arbabi, A. Faraon, *ACS Photonics* **2019**, 6, 2712.

[44] H. Li, D. B. Phillips, X. Wang, Y.-L. D. Ho, L. Chen, X. Zhou, J. Zhu, S. Yu, X. Cai, *Optica* **2015**, 2, 547.

[45] H. Sroor, Y.-W. Huang, B. Sephton, D. Naidoo, A. Vallés, V. Ginis, C.-W. Qiu, A. Ambrosio, F. Capasso, A. Forbes, *Nature Photonics* **2020**, 14, 498.

[46] J. Yang, S. Gurung, S. Bej, P. Ni, H. W. H. Lee, *Reports on Progress in Physics* **2022**, 85, 036101.

Figures：

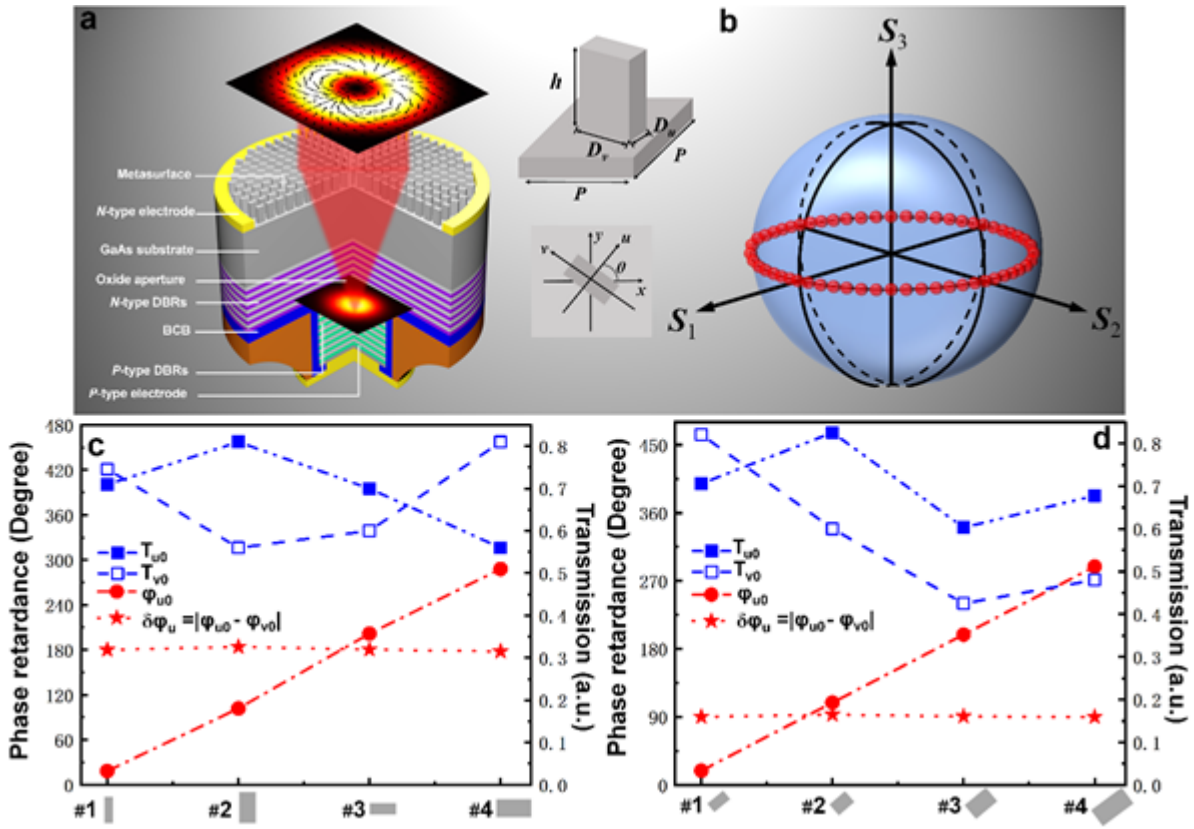

Figure 1. Vector beam generation and manipulation enabled by on-chip integration of birefringent metasurface. a, the schematic illustration of a Meta-VCSEL to create complex vectorial fields with well-defined wavefronts, the inset shows the employed meta-atom with rectangular cross-section. b, the achievable polarization states on the Poincaré sphere in this example by operating the anisotropic meta-atoms as nano half-waveplates. Simulated complex transmission coefficients of meta-atoms as the building blocks of the metasurface at the lasing wavelength of 977 nm, in which the selected elements maintain the fixed phase difference between the two eigen-polarization channels with $\Delta\varphi = |\varphi_{u0} - \varphi_{v0}| = \pi$ (c) or $\pi/2$ (d). In this way, the selected meta-atoms can work as nano half-waveplates (c) or quarter-waveplates (d) with controllable propagation phase in the complete 2π range, respectively.

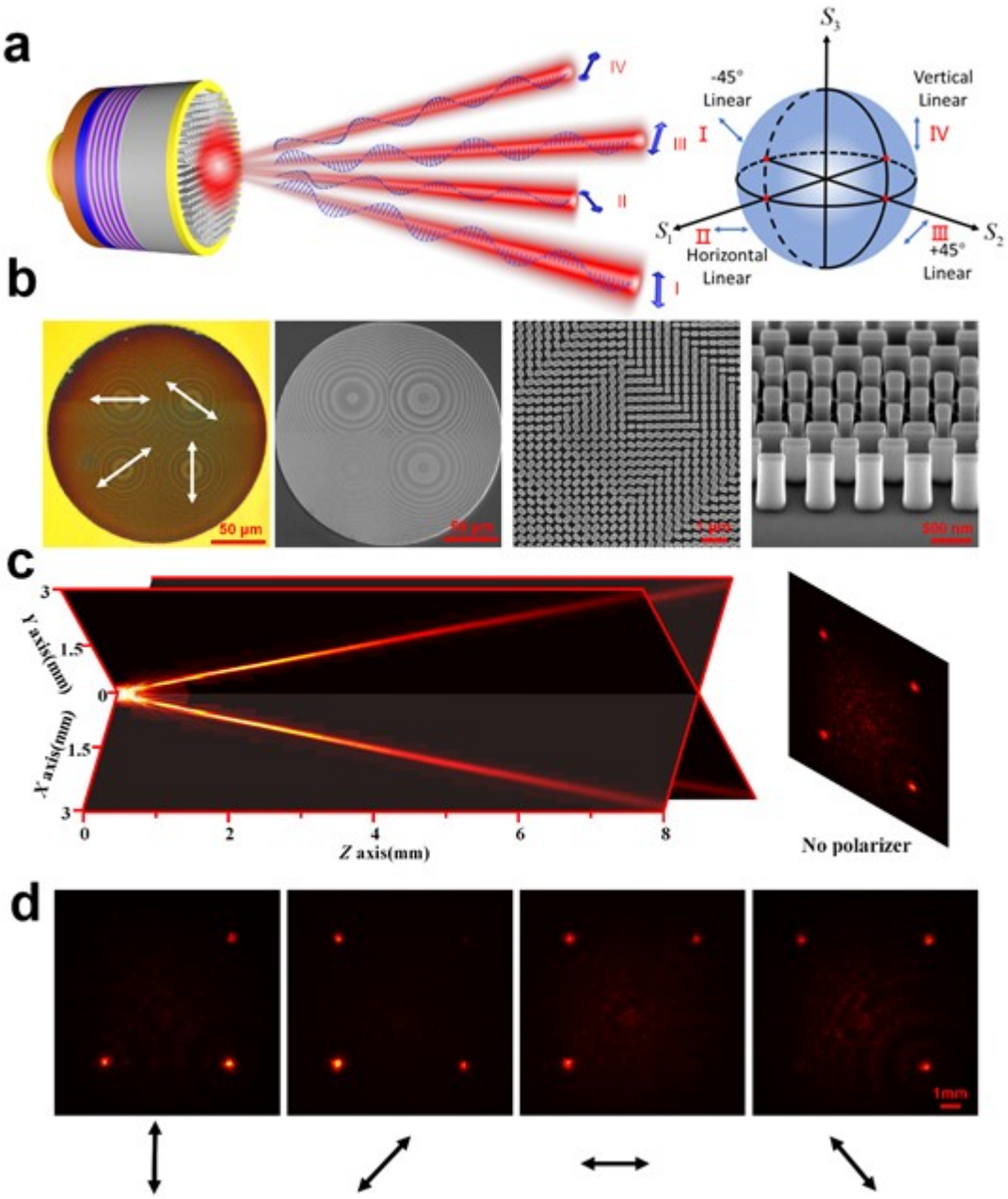

Figure 2. Directional generation of multibeam with specified polarizations. a, Conceptual design of multibeam generations with well-defined directionalities and polarization states based on a metasurface integrated VCSEL. As a proof of concept, four different linear polarizations (0^o, 45^o, 90^o, and 135^o) are created. b, Optical and SEM images show the high-quality fabrication of the spatially segmented metasurface. c, d, the specified SOPs of the generated beams are determined by

measuring the polarization-resolved intensity distributions in the *x*-*y* plane at Z = 1.5 cm using a polarization analyzer. which exhibit large polarization extinction ratios. The white arrows represent the polarization direction of the transmitted beam.

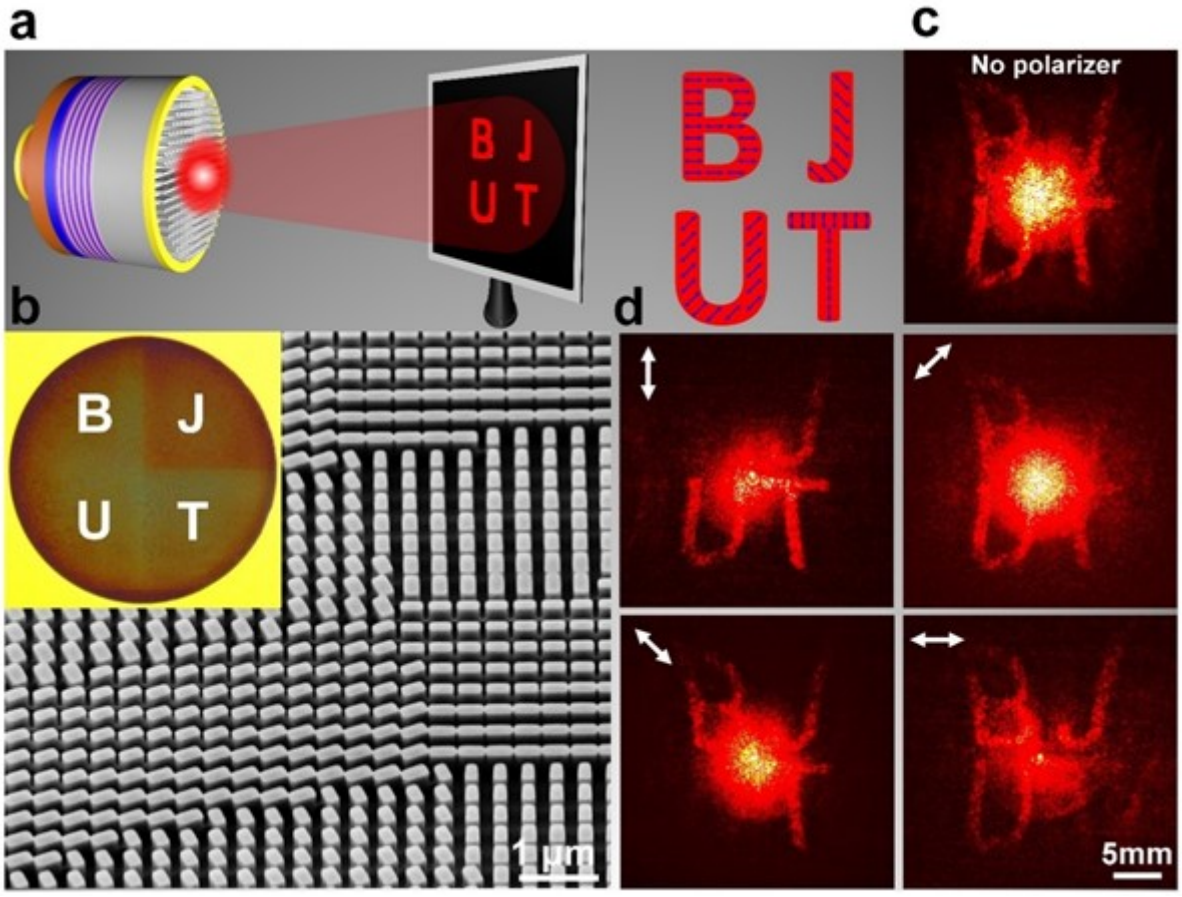

Figure 3. On-chip vectorial holographic display. a, schematic of the concept for on-chip vectorial holographic display, which can construct the letters “B”, “J”, “U”, and “T” with specified polarizations in the far-field. b, The SEM image of the integrated vectorial metasurface hologram. The inset shows an optical image of the whole area of the metasurface, which is spatially divided into four sectors to display the encoded images, respectively. c, the designed four letters can be observed simultaneously without any polarization analyzers. d, the pre-defined SOPs of the obtained vectorial

holography were verified by selectively filtering out the constructed image using a polarization analyzer rotated at different angles. The white arrows indicate the transmission axis of the polarizer.

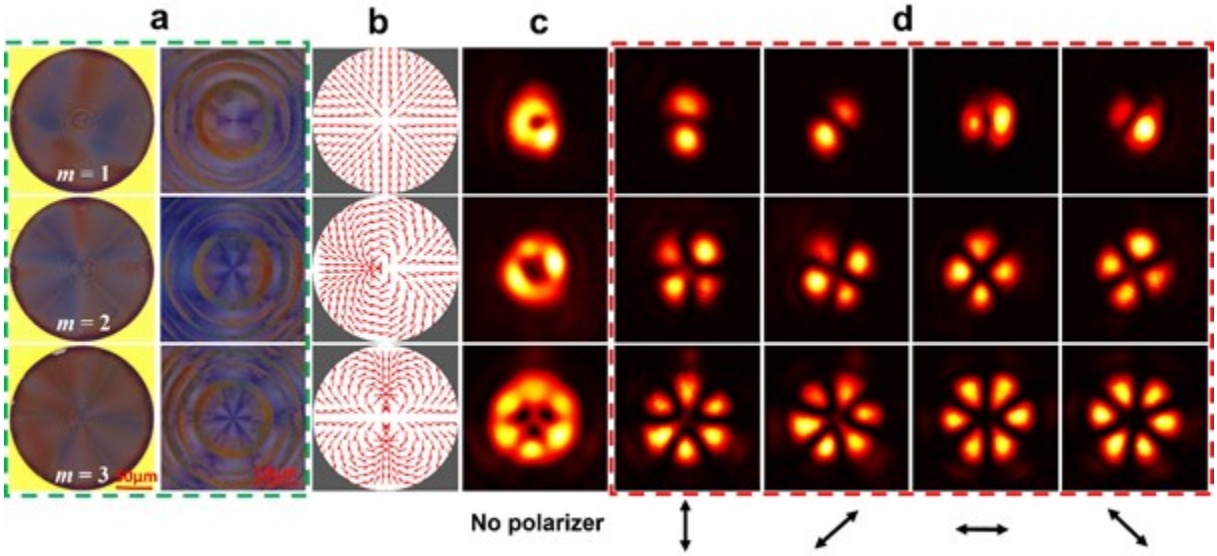

Figure 4. Generations of vector vortex beams. a. optical images of the integrated metasurface for VVBs generations. b, polarization distributions of the designed metasurface vortex waveplates of different polarization orders (m = 1, 2, and 3) with a fixed initial phase ($\varphi = 0$). c, beam profiles measured at Z = 4 mm without the use of polarization analyzer show doughnut shaped distribution with intensity null in the center, confirming the polarization singularities. d summarizes the recorded spatial-resolved polarization profiles of the beams, where two-lobe, four-lobe, and six-lobe patterns in orthogonal directions with respect to the polarizer can be observed, respectively, confirming the generations of radial vector beams of m = 1, 2, and 3, respectively.

The table of contents:

On-chip generation and manipulation of vector beams are demonstrated by monolithically integrating vectorial metasurfaces with standard Vertical Cavity Surface-Emitting Lasers (VCSELs). The developed approach enables a powerful tool to structure the complex wavefronts of a VCSEL in an ultracompact way, providing the access to previously unattainable both phase and polarization degrees of freedom.

Keywords: Metasurface; Vector beams; VCSELs; on-chip integration

Title: Metasurface enabled On-Chip Generation and Manipulation of Vector Beams from Vertical Cavity Surface-Emitting Lasers

Pan Fu, Pei-Nan Ni, Bo Wu, Xian-Zhi Pei, Qiu-Hua Wang, Pei-Pei Chen, Chen Xu, Qiang Kan*,Wei-Guo Chu* and Yi-Yang Xie**

ToC figure: